

Topological Well-Composedness and Glamorous Glue: A Digital Gluing Algorithm for Topologically Constrained Front Propagation

Nicholas J. Tustison, Brian B. Avants, Marcelo Siqueira, and James C. Gee

Abstract— We propose a new approach to front propagation algorithms based on a topological variant of *well-composedness* which contrasts with previous methods based on *simple point* detection. This provides for a theoretical justification, based on the digital Jordan separation theorem, for digitally “gluing” evolved well-composed objects separated by well-composed curves or surfaces. Additionally, our framework can be extended to more relaxed topologically constrained algorithms based on *multisimple points*. For both methods this framework has the additional benefit of obviating the requirement for both a user-specified connectivity and a topologically-consistent marching cubes/squares algorithm in meshing the resulting segmentation.

Index Terms— digital Jordan separation theorem, front propagation, marching cubes, simple point, topological well-composedness

I. INTRODUCTION

The exploration of topological concepts for digital image analysis algorithms dates back to the pioneering work of the late Azriel Rosenfeld who coined the phrase *digital topology*. Given the digitization of structures of interest via the imaging process whose continuous topology is known a priori, digital topological considerations for image segmentation algorithms continue to be of significant research interest. Although general variational approaches to topology constrained front propagation include the work of [1], [2], [3], [4] in this work, we focus on those methods based on the fundamental digital topology concept of *simple points* [5] which characterizes the local digital topology of a specified voxel based on the foreground/background identity of the immediate voxel neighborhood given a user-specified connectivity relation. Exemplary methods include those of [6], [7].

We propose an extension to the digital concept of well-composedness [8], [9], [10], which we denote as *topological well-composedness*, for strictly maintaining the topology of the evolving digital fronts similar to the simple point approach of Han et al. [6]. However, since our topology constraint employs well-composedness, we can utilize the digital Jordan separation theorem (DJST) [10] to ‘glue’ digital objects separated by well-composed curves or surfaces. The well-composed hypersurface forming the boundaries between objects, i.e. the digital gluing layer, has the potential to provide further interesting shape-based analysis of such boundaries. This framework can also be extended to more relaxed topology constrained methods such as that of [7]. Regardless of topology constraint, this framework does not require the user to specify a connectivity relation nor the use of connectivity consistent marching cubes/squares (CCMC) algorithms (e.g. [11], [6], [12]) to handle ambiguous tiling cases. As a practical contribution, we have integrated our method in the fast marching image filter of the Insight Toolkit of the National Institutes of Health (based on the algorithm given in [13]) which we plan to provide to the open source community.

II. DIGITAL TOPOLOGY FOR CONSTRAINING FRONT PROPAGATION

The following core digital topological concepts are briefly reviewed to better contextualize our contribution:

- simple points [14], [5], [15],
- multisimple points [7],
- well-composedness [8], [9], and
- topological well-composedness.

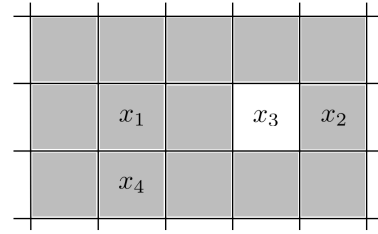


Fig. 1: Illustration of simple and non-simple (i.e. critical) points for a 2-D binary image. Note that X is represented by the grey squares and \bar{X} by the white squares. x_1 , x_2 , and x_3 are not simple points whereas x_4 is a simple point. Changing x_1 or x_2 to background would create a hole or eliminate a handle, respectively, while changing x_3 to foreground would fill a hole. However, changing only x_4 does not violate digital topology.

Each of these concepts is based on sets represented by binary images. A binary image, I , is composed of foreground and background components, represented respectively by X and \bar{X} . Given arbitrary I , a connectivity relation is specified to avoid topological ambiguities. These connectivity relations are denoted as $(6, 18)$, $(6, 26)$, $(18, 6)$, or $(26, 6)$ in 3-D or $(4, 8)$ and $(8, 4)$ in 2-D where the first and second numbers specify the adjacency relation of points in X and \bar{X} , respectively [14].

In addition, definitions concerning local neighborhood relationships are necessary for further discussion of certain concepts. Given a voxel $x \in X$, the n -neighborhood of x is denoted as $N_n(x)$ and $N_n^*(x) = N_n(x) \setminus \{x\}$. Related is the concept of the *n -geodesic neighborhood* of x ([5], [6]):

Definition The n -geodesic neighborhood of x with respect to X of order k (denoted by $N_n^k(x, X)$) is defined recursively as follows: $N_n^k(x, X) = \cup \{N_n(y) \cap N_M^*(x) \cap X, y \in N_n^{k-1}(x, X)\}$ with $N_n^1(x, X) = N_n^*(x) \cap X$ where $M = 8$ in 2-D and $M = 26$ in 3-D.

We also denote the number of n -connected components of X as $C_n(X)$ and the number of n -connected components of $X \setminus \{x\}$ which exhibit n -adjacency to x as $C_n(X, x)$.

A. Simple Points

A *simple point* in I can be informally defined as a voxel which can switch from background to foreground or vice versa without altering the existing topology of I [5], [15] (see Fig. 1). This concept is important for defining topology preserving transformations—specifically for thinning and skeletonization algorithms [16], [14] and front propagation [6], [17], [7].

Bertrand proposed the *topological numbers* $T_n(x, X)$ and $T_{\bar{n}}(x, \bar{X})$ to characterize the topology of the point x with respect to X and \bar{X} given a specified adjacency relation (n, \bar{n}) [18] which can be defined in terms of the geodesic neighborhood of x :

Definition

$$T_4(x, X) = \#(C_4(N_4^2(x, X)))$$

$$T_8(x, X) = \#(C_8(N_8^2(x, X)))$$

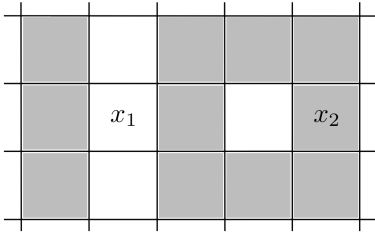


Fig. 2: Illustration of multisimple and non-multisimple points for a 2-D binary image. Note that X is represented by the grey squares and \bar{X} by the white squares. Whereas x_1 is a multisimple point ($T_n^+ = T_n = 2$), x_2 is not ($T_n^+ = 1 \neq T_n = 2$).

in 2-D where ‘#’ denotes the cardinality of a set and

$$\begin{aligned} T_6(x, X) &= \#(C_6(N_6^2(x, X))) \\ T_{6^+}(x, X) &= \#(C_6(N_6^3(x, X))) \\ T_{18}(x, X) &= \#(C_{18}(N_{18}^2(x, X))) \\ T_{26}(x, X) &= \#(C_{26}(N_{26}^1(x, X))) \end{aligned}$$

in 3-D where ‘6⁺’ is used for (6, 18) connectivity and ‘6’ is used for (6, 26) connectivity.

These topological numbers are useful for identifying isolated, interior, and junction points in addition to simple points [5], the latter being characterized by the necessary and sufficient condition $T_n(x, X) = T_{\bar{n}}(x, \bar{X}) = 1$.

B. Multisimple Points

Ségonne extended the concept of topological numbers to characterize multisimple points [7]:

Definition A point in I is multisimple if it can be added or removed without changing the number of handles of X and \bar{X} .

Multisimple points are similarly characterized by their *extended topological numbers* $T_n^+(x, X)$ and $T_{\bar{n}}^+(x, \bar{X})$. These numbers are determined by the set of connected components with respect to both X and \bar{X} , denoted by $C_n(x, X)$ and $C_{\bar{n}}(x, \bar{X})$, respectively, such that

$$T_n^+(x, X) = |C_n(x, X)| \quad \text{and} \quad T_{\bar{n}}^+(x, \bar{X}) = |C_{\bar{n}}(x, \bar{X})|. \quad (1)$$

Multisimple points can then be defined formally as those points satisfying the following relations:

$$T_n^+(x, X) = T_n(x, X) \quad \text{and} \quad T_{\bar{n}}^+(x, \bar{X}) = T_{\bar{n}}(x, \bar{X}). \quad (2)$$

A sample 2-D binary image is given in Fig. 2 which illustrates the difference between multisimple points and non-multisimple points. By restricting evolution of the dynamic front to multisimple points, as opposed to simple points, Ségonne’s method allows objects to merge and split without creating handles.

C. Well-Composedness

For $n = \{2, 3\}$, an n -D binary digital image, I , is said to be well-composed [8], [9] if and only if the continuous analog of the digital boundary between X and \bar{X} in I is a $(n - 1)$ -D manifold [10]. Informally, a well-composed image is one with only face connectedness between points in both X and \bar{X} , i.e. adjacency relations for X and \bar{X} are (6, 6) for 3-D sets and (4, 4) for 2-D sets such that I is absent of any so-called critical configurations, ξ , illustrated for 2-D and 3-D images in Fig. 3. Thus,

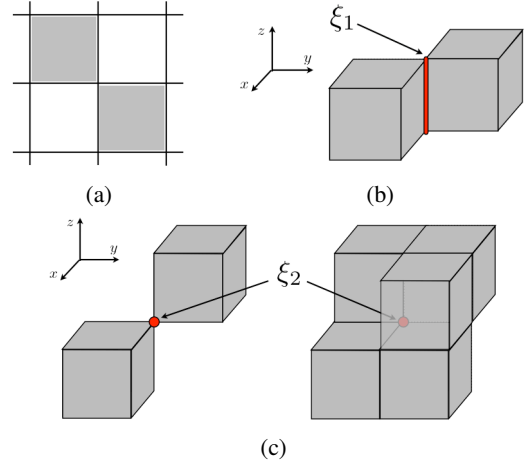


Fig. 3: Critical configurations characterizing non well-composed images in both 2-D and 3-D in local 2^D neighborhoods. (a) The 2-D critical configuration is due to an 8-adjacency relation. In 3-D (b) the critical configuration ξ_1 is due to an 18-adjacency relation and (c) the critical configuration ξ_2 is due to a 26-adjacency relation. The repairing algorithms of [10], [19] eliminate these local critical configurations (and their rotational and reflection variants) to make an image well-composed.

well-composedness obviates the requirement of specifying one of the standard connectivity relations of (6, 18), (6, 26), (18, 6), and (26, 6) in 3-D or connectivities of (4, 8) and (8, 4) in 2-D for establishing the topology of I . Well-composedness implies important topological and geometrical properties which simplifies many algorithms such as marching cubes/squares [20], various thinning algorithms, and Euler characteristic computation. The “repairing” algorithms given in [10], [19], [21] are used to make 2-D and 3-D binary images well-composed by optimally eliminating such critical configurations.

D. Topological Well-Composedness

As described previously, the simple point criterion can be used to constrain the topology of an evolving digital front. In contrast, the well-composedness criteria, as initially defined, is insufficient for such a task. Towards this end, we extend the concept of well-composedness to its topological variant by incorporating the 2-D and 3-D topological critical configurations illustrated in Fig. 4 where only the center voxel and its immediate face-connected neighbors are considered. Note that 8-connected neighbors in 2-D and 18- and 26-connected neighbors in 3-D are handled by the well-composedness criteria given in Fig. 3. Those voxels which satisfy both the well-composedness and corresponding topological criteria are designated *topologically well-composed points*.

III. TOPOLOGICALLY CONSTRAINED WELL-COMPOSED FRONT PROPAGATION

A. Strict Topology Preservation

Constraining the evolution of the digital front to either simple or topologically well-composed points, one can strictly preserve the initial topological configuration during the transformation. Visual comparison of our method with the strict preserving topology approach of Han et al. [6] is given in Fig. 5 where detection of simple points along the dynamic front maintains the topology of the original level set configuration. Starting with seven well-composed seed objects placed in the center of the seven canine

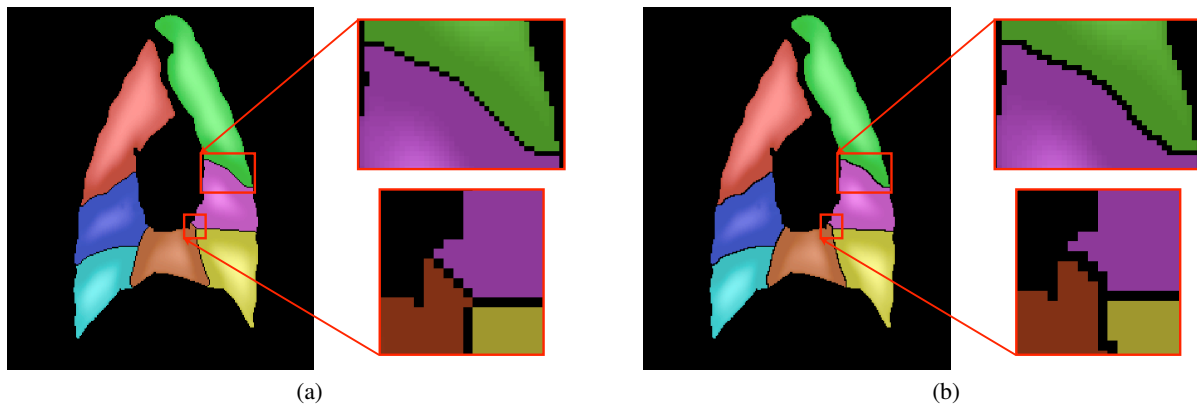


Fig. 5: Strict topology preserving fast marching segmentation of the seven canine lobes. (a) The results of the topology preserving level set method of Han et al. [6] using a (4, 8) adjacency relationship. These results can be compared with (b) our approach using topological well-composedness for constraining level set evolution which results in a binary sets exhibiting (4, 4) adjacency.

lobes, the dynamic front evolves while strictly maintaining the initial topological configuration. Fig. 5(a) shows the resulting configuration where we have labeled the different connected components with different color labels. We have also zoomed in on two interfaces to illustrate the characteristic separation demonstrating the (4, 8) adjacency relation. For comparison, we provide the results using our approach in Fig. 5(b) where the resulting well-composed binary set exhibits (4, 4) adjacency.

B. Digitally Gluing Genus Zero Well-Composed Binary Sets

1) Glamorous Glue and the Digital Jordan Separation Theorem:

Following evolution using strict topology preservation of the initial configuration via topological well-composedness, neighboring well-composed genus zero seed objects can be digitally “glued” along the well-composed hypersurface interface to create a single, well-composed genus zero object. This gluing operation creates a well-composed manifold that, for certain applications, can be construed as having anatomical meaning for further shape analysis (e.g. the fissures separating the lobes of the lungs). This is possible since the DJST applies to well-composed sets [10].

The Jordan curve theorem, originally formalized for simple closed curves in the \mathbf{R}^2 plane, also extends to curves on a sphere. The Jordan separation theorem (JST) on the sphere says that a surface homeomorphic to a sphere, i.e. surface with genus zero, may be separated into two objects by a simple, continuous, closed curve (a Jordan curve) drawn along the surface [22]. Note that the two separated objects are topologically equivalent—they both have the topology of a plane. Similarly, any two genus zero objects are topologically equivalent. That is, there exists a homeomorphism between them. The JST for the continuous world has a digital analog [10] where the spherical object is represented as a dense volume of voxels which are hole- and loop-free. Latecki has also shown that the DJST holds true for well-composed objects [10]. These results enable a concrete application of this theorem to the case of well-composed genus zero digital objects.

A corollary of this theorem is that we can glue two distinct genus zero surfaces, X_A and X_B , by a simple set of operations, to create a new genus zero surface. The crux of the argument is that a Jordan curve separates a genus zero object into two components with identical planar topology which can then be homeomorphically mapped to the boundaries of other similarly separated components, also with identical planar topology, derived from application of the Jordan curve theorem. Fig. 6 shows the JST applied to two genus

zero objects. To show this corollary more clearly, we describe the proof by construction which is closely connected to the Glamorous Glue algorithm itself which is given in Algorithm 1.

Corollary 3.1: (Gluing Corollary for the JST) Two distinct genus zero objects may be glued along a Jordan curve to form a new genus zero object.

Proof: First, we perform a separation along each surface by drawing a Jordan curve, i.e. we draw J_A on X_A and J_B on X_B . Note that each J forms the boundary of a well-composed manifold such that each J has an “interior” and an “exterior”. Arbitrarily, we take the interior to be the smallest area component after separation. Second, we replace the interior of J_A with the exterior of J_B by gluing these pieces along J_A (without loss of generality). Note that as each of these objects are topologically equivalent, J_B may be homeomorphically mapped to J_A or vice versa. Then, due to identical planar topology of the interior and exterior components of both J_A and J_B , the resulting surface is genus zero. ■

2) *Quantitative Comparison:* Although the techniques discussed in previous sections are generally applicable, much of the motivation for this work and related work (e.g. [23], [6], [17], [24]) has been towards retrospective correction of brain segmentation to ensure correct topology of the final segmentation. Since with strict topology preservation the initial topological configuration is equal to the final topological configuration, only initialization with a single initialization seed object is possible. However, using the GG algorithm one can initialize the topological correction with anatomically meaningful well-composed genus zero objects (e.g. the brain lobes). These lobes can then be glued together to create a single genus zero object. *Thus, one obtains the results yielded by earlier strategies while also maintaining potentially anatomically meaningful subdivisions.*

Image data (NA0) from the Non-Rigid Image Registration Evaluation Project (NIREP) consisting of 16 labeled human brain volumes were used for quantitative comparison.¹ In Step 1 of Algorithm 1, we assumed an initialization was given. However, in general, determining an optimal initialization for finding the globally optimal fit of a genus zero segmentation to an arbitrary topology target segmentation is an unsolved problem. Since different strategies for initialization have the potential of finding different local minima, specific strategies are needed for specific applications.

Based on brain anatomy and in order to motivate the GG algorithm,

¹<http://www.nirep.org>

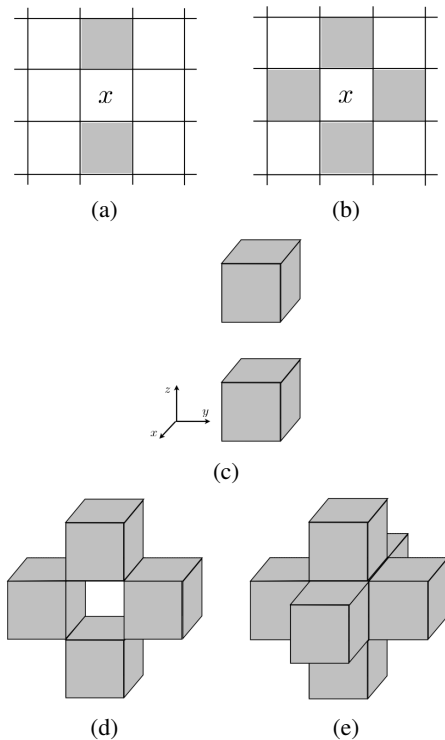


Fig. 4: (a)–(e) Additional critical configurations (and their rotational invariants) for topological well-composedness for a specific voxel in \bar{X} and its immediate face-connected voxel neighborhood. Changing the voxel’s membership from \bar{X} to X would change the topology of I . Note that the membership (in X or \bar{X}) of the neighborhood voxels identified by a corner or edge connectivity is unimportant as these cases are handled by the identification of the well-composedness critical configurations illustrated in Fig. 3.

we opted to initialize the GG algorithm with four initialization seed objects corresponding to the four major lobes in each of the 16 NIREP image data: frontal, temporal, parietal, and occipital. These four lobar seed objects are found by extracting the largest possible cube-like set of voxels accommodated within each lobe. This initialization approach is illustrated in Fig. 7(a) where we have rendered the translucent white matter of the right hemisphere of one of the NAO data sets along with the four seed objects. Each of the four seed objects has been rendered with a different color label (red \rightarrow frontal lobe, green \rightarrow parietal lobe, blue \rightarrow temporal lobe, and purple \rightarrow occipital lobe). These four seed objects evolve as described in Algorithm 1 followed by construction of the gluing layer seen in Fig. 7(d).

For comparison, we initialize with a single object (similar to [6]) in the occipital lobe since it is the most convoluted and gives the best overall comparative performance. We denote this strategy as ‘Simple.’ The voxel-wise difference and error percentages between the actual segmentation and our two retrospective corrections are given in Fig. 8. Both initialization strategies produce a final genus zero object representing the white matter for each of the 16 data. However, not only does our approach maintain anatomically meaningful subdivisions, but the inherent split-and-merge approach minimizes the segmentation error for all lobes collectively and for all but the parietal lobe individually over all 16 NIREP data.

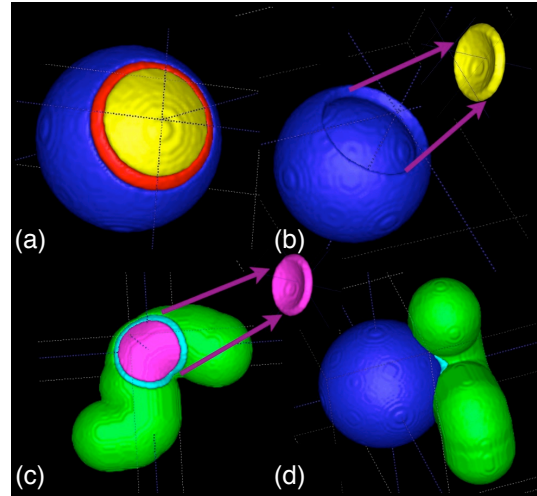


Fig. 6: Illustration of the continuous Jordan separation theorem. (a) A genus zero object, X_A , is shown with a Jordan curve, J_A , drawn along the surface. The interior of the J_A is painted yellow and has planar topology by construction. (b) The separation of the interior of J_A results in two planar objects. (c) A similar operation is performed on a second genus zero object, X_B , with its corresponding Jordan curve, J_B resulting in two planar objects. (d) The gluing corollary of the Jordan separation theorem indicates that we may replace the original interior of J_A with the topologically equivalent exterior of J_B resulting in a single genus zero object with a different shape from the original.

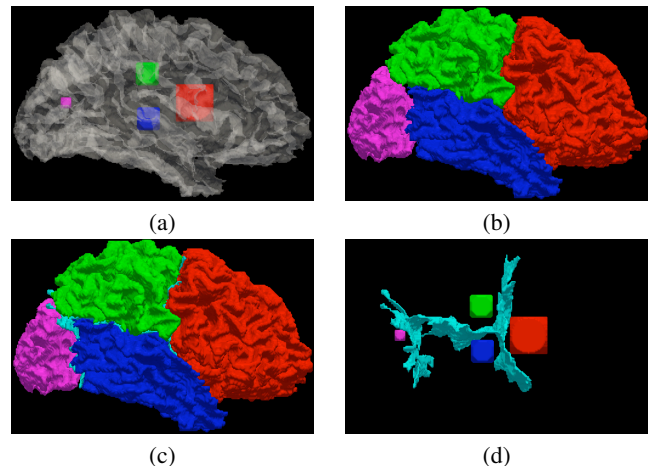


Fig. 7: Glamorous Glue applied to brain segmentation results. (a) Initialization begins with four well-composed, genus zero objects, each with a distinct label (red \rightarrow frontal lobe, green \rightarrow parietal lobe, blue \rightarrow temporal lobe, purple \rightarrow occipital lobe). (b) After deformation, the four lobes are separated by a digital planar interface such that the original topology is maintained. (c) Applying the gluing step produces a single segmentation with the correct topology. (d) The final gluing layer is shown in isolation with the original initialization objects.

Algorithm 1 Glamorous Glue

- 1: Place multiple, well-composed, genus zero seed objects within the target segmentation.
 - 2: Create the initial front using a signed distance transform on the seed objects.
 - 3: Evolve the dynamic fronts according to the governing region growing/shrinking propagation equations while strictly preserving the topology of the initial configuration. Note that evolution of each seed object must be carried out until propagation halts due to topology preserving constraints.
 - 4: **while** there exists > 1 genus zero object **do**
 - 5: Determine the connected components of all the unlabeled interfaces between the evolved, well-composed, genus zero objects.
 - 6: Isolate the largest unlabeled interface. This interface is defined by the local 8- (2-D) or 26- (3-D) neighborhood containing only points $x_A \in X_A$ and $x_B \in X_B$ where X_A and X_B are the two genus zero objects on either side of the interface.
 - 7: Locate a *legal gluing position* at one voxel along the interface. A *legal gluing position* is a point $x \in \bar{X}$ on the interface between X_A and X_B that conforms locally to the JST and does not violate well-composedness. Quantitative criterion for selecting among candidate legal positions may be used, such as selecting the legal gluing position that is maximally far from the image background.
 - 8: Evolve the seed object within the interface between X_A and X_B using the TWC strict topology preserving level set method. The advancing front terminates at either an illegal gluing position or at a position y where $N(y) \cap X_A = \emptyset$ or $N(y) \cap X_B = \emptyset$ or $N(y) \cap X_C \neq \emptyset$ where X_C is a possible third genus zero well-composed object within the target segmentation. The boundary of the resulting grown region constitutes the digital Jordan curve along which we have the final gluing of X_A and X_B .
 - 9: **end while**
-

C. ‘No Handles’ Topology Constraint

Not only does our framework accommodate strict topology preservation but one can also adopt the multisimple point, multiple object initialization [7] for a more relaxed topology constraint where fronts can split and merge but not form handles. This is done by relaxing the topological well-composed criteria illustrated in Fig. 4 to allow merging separate connected component objects or splitting a single connected object which we denote *relaxed topological well-composedness*. All that is required is maintaining a connected component label map and consulting the map during evolution.

In addition, one benefit with our approach is that CCMC algorithms are not required to produce a topologically consistent meshing from the segmentation results. We compare both 1) the relaxed topological well-composed approach with the analogous approach of [7] and 2) the topologically consistent meshing of the resulting segmentation by both methods to segmentation of the white matter of the BrainWeb 20 image database [25] of the right hemisphere. After extracting the right hemisphere of the white matter for all 20 subjects, ~ 2400 initialization points are randomly placed in the white matter common to all 20 subjects. For each method we calculate the average and standard deviation of the resulting genus as determined by a publicly available, well-vetted, standard marching cubes implementation² Although for typical surfaces the genus is restricted to positive integer values, non-orientable surfaces (which can result from application of the original

²<http://www.vtk.org/doc/nightly/html/classvtkMarchingCubes.html>

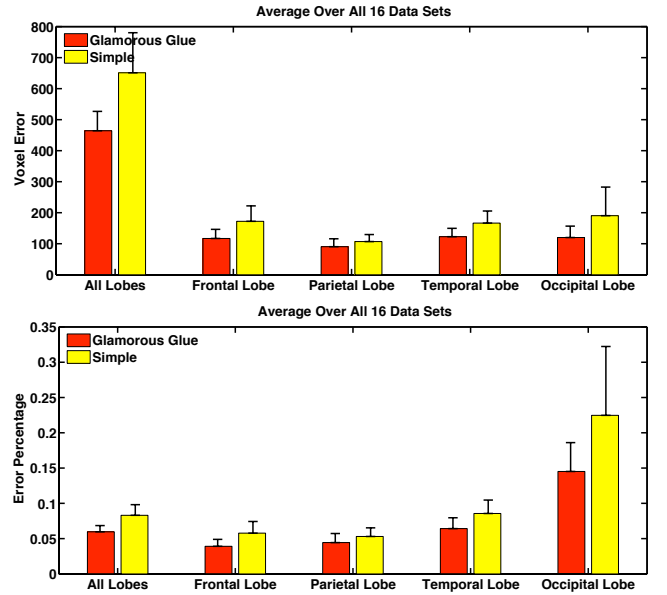


Fig. 8: Comparative performance assessment of GG (red bars) and Simple approach (yellow bars) averaged over all 16 data sets with error bars showing one standard deviation. The top panel shows the average voxel-wise difference between the target segmentation and the segmentation produced by the two algorithms for the 16 NIREP image data. The bottom panel illustrates the difference as the error percentage. Corresponding p -values are $p_{All} = 0.0018$, $p_{Frontal} = 0.047$, $p_{Parietal} = 0.116$, $p_{Temporal} = 0.0132$, and $p_{Occipital} = 0.026$.

TABLE I: ‘No Handles’ Topology Method Comparison

| Method | Genus | Voxel Difference |
|------------------------|--------------------|---------------------|
| No Topology Constraint | 508 \pm 210 | 0.9999 \pm 0.0002 |
| MP _(6,18) | 10.8 \pm 4.1 | 0.994 \pm 0.002 |
| MP _(18,6) | 19.6 \pm 6.5 | 0.992 \pm 0.003 |
| MP _(6,26) | -188.6 \pm 203.2 | 0.993 \pm 0.002 |
| MP _(26,6) | 23.8 \pm 9.85 | 0.991 \pm 0.003 |
| RTWC | 0 \pm 0 | 0.990 \pm 0.002 |

MP = Multisimple Point

RTWC = Relaxed Topological Well-Composedness

(\cdot, \cdot) denotes connectivity

marching cubes algorithm) result in negative genus values.

Consistent with expectations, only our method yielded the correct genus for all 20 BrainWeb subjects with the standard marching cubes algorithm (results given in Table I). Although our method yields a topologically consistent solution, it will also be noted that voxel difference ratio is least for our method. This is readily explained when one considers that relaxed topological well-composedness, by permitting only face-connectedness, yields the most conservative solution.

IV. CONCLUSIONS

In conclusion, we presented a novel framework for topology constrained front propagation methods which relies on a substitution of a criterion of topological well-composedness for the related criterion of simple and multisimple points which theoretically justifies our Glamorous Glue algorithm. This justification stems from application of the digital Jordan separation theorem which allows for digitally gluing independent genus zero objects to form new, unified genus

zero objects. An additional advantage is the elimination of CCMC algorithmic requirements for meshing the resulting segmentation.

REFERENCES

- [1] T. C. Cecil, "Numerical methods for partial differential equations involving discontinuities," Ph.D. dissertation, University of California, Los Angeles, 2003.
- [2] O. Alexandrov and F. Santosa, "A topology-preserving level set method for shape optimization," *Journal of Computational Physics*, vol. 204, no. 1, pp. 121–130, 2005.
- [3] G. Sundaramoorthi and A. Yezzi, "Global regularizing flows with topology preservation for active contours and polygons," *IEEE Trans Image Process*, vol. 16, no. 3, pp. 803–812, Mar 2007.
- [4] C. L. Guyader and L. A. Vese, "Self-repelling snakes for topology-preserving segmentation models," *IEEE Trans Image Process*, vol. 17, no. 5, pp. 767–779, May 2008. [Online]. Available: <http://dx.doi.org/10.1109/TIP.2008.919951>
- [5] G. Bertrand, "Simple points, topological numbers and geodesic neighborhoods in cubic grids," *Pattern Recognit. Lett.*, vol. 15, no. 10, pp. 1003–1011, 1994.
- [6] X. Han, C. Xu, and J. Prince, "A topology preserving level set method for geometric deformable models," *IEEE Trans. Pattern Analysis and Machine Intelligence*, vol. 25, no. 6, pp. 755–768, 2003.
- [7] F. Ségonne, "Active contours under topology control—genus preserving level sets," *Int. J. Comput. Vision*, vol. 79, no. 2, pp. 107–117, 2008.
- [8] L. Latecki, U. Eckhardt, and A. Rosenfeld, "Well-composed sets," *Computer Vision and Image Understanding*, vol. 61, pp. 70–83, 1995.
- [9] L. J. Latecki, "3D well-composed pictures," *Graphical Models and Image Processing*, vol. 59, no. 3, pp. 164–172, 1997.
- [10] L. Latecki, *Discrete Representation of Spatial Objects in Computer Vision*. Springer, 1998.
- [11] J.-O. Lachaud and A. Montanvert, "Continuous analogs of digital boundaries: a topological approach to iso-surfaces," *Graphical models*, vol. 62, no. 3, pp. 129–164, 2000.
- [12] T. Lewiner, H. Lopes, A. W. Vieira, and G. Tavares, "Efficient implementation of marching cubes' cases with topological guarantees," *Journal of graphics, gpu, and game tools*, vol. 8, no. 2, pp. 1–15, 2003.
- [13] J. A. Sethian, *Level Set Methods and Fast Marching Methods: Evolving Interfaces in Computational Geometry, Fluid Mechanics, Computer Vision, and Materials Science*. Cambridge University Press, 1999.
- [14] T. Y. Kong and A. Rosenfeld, "Digital topology: Introduction and survey," *Computer Vision, Graphics, and Image Processing*, vol. 48, pp. 357–393, 1989.
- [15] G. Bertrand, "A boolean characterization of three-dimensional simple points," *Pattern Recognit. Lett.*, vol. 17, pp. 115–124, 1996.
- [16] A. Rosenfeld, "Connectivity in digital pictures," *J. ACM*, vol. 17, pp. 146–160, 1970.
- [17] P.-L. Bazin and D. L. Pham, "Topology-preserving tissue classification of magnetic resonance brain images," *IEEE Trans Med Imaging*, vol. 26, no. 4, pp. 487–496, Apr 2007. [Online]. Available: <http://dx.doi.org/10.1109/TMI.2007.893283>
- [18] G. Bertrand and G. Malandain, "A new characterization of three-dimensional simple points," *Pattern Recogn. Lett.*, vol. 15, no. 2, pp. 169–175, 1994.
- [19] M. Siqueira, L. J. Latecki, N. Tustison, J. Gallier, and J. Gee, "Topological repairing of 3-D digital images," *Journal of Mathematical Imaging and Vision*, vol. 30, no. 3, pp. 249–274, March 2008.
- [20] W. E. Lorensen and H. E. Cline, "Marching cubes: A high resolution 3d surface construction algorithm," *Computer Graphics*, vol. 21, no. 4, pp. 163–169, 1987.
- [21] N. J. Tustison, M. Siqueira, and J. C. Gee, "Well-composedness and the topological repairing of digital images," *The Insight Journal*, 2007. [Online]. Available: <http://hdl.handle.net/1926/470>
- [22] M. Nakahara, *Geometry, Topology and Physics*. Taylor and Francis, 2003.
- [23] D. W. Shattuck and R. M. Leahy, "Automated graph-based analysis and correction of cortical volume topology," *IEEE Trans Med Imaging*, vol. 20, no. 11, pp. 1167–1177, Nov 2001. [Online]. Available: <http://dx.doi.org/10.1109/42.963819>
- [24] P.-L. Bazin and D. L. Pham, "Homeomorphic brain image segmentation with topological and statistical atlases," *Med Image Anal.*, vol. 12, no. 5, pp. 616–625, Oct 2008. [Online]. Available: <http://dx.doi.org/10.1016/j.media.2008.06.008>
- [25] B. Aubert-Broche, M. Griffin, G. B. Pike, A. C. Evans, and D. L. Collins, "Twenty new digital brain phantoms for creation of validation image data bases," *IEEE Trans Med Imaging*, vol. 25, no. 11, pp. 1410–1416, Nov 2006. [Online]. Available: <http://dx.doi.org/10.1109/TMI.2006.883453>